AD_____
(Leave blank)

Award Number: W81XWH-12-2-0047

TITLE: Engineering of Paraoxonases for Pre- and Post-treatment of Intoxication by a Broad Spectrum of Nerve Agents and Pesticides

PRINCIPAL INVESTIGATOR: Dan Tawfik (Ph.D.)

CONTRACTING ORGANIZATION: Weizmann Institute of Science, Rehovot 76100, Israel

REPORT DATE: August 2014

TYPE OF REPORT: Final

PREPARED FOR: U.S. Army Medical Research and Materiel Command
Fort Detrick, Maryland 21702-5012

DISTRIBUTION STATEMENT:

√ Approved for public release; distribution unlimited

REPORT DOCUMENTATION PAGE

Form Approved
OMB No. 0704-0188

1. REPORT DATE *(DD-MM-YYYY)*	2. REPORT TYPE	3. DATES COVERED *(From - To)*
August 2014	Final Report	7-May-2012 to 6-May-2014

4. TITLE AND SUBTITLE
Engineering of Paraoxonases for Pre- and Post-treatment of Intoxication by a Broad Spectrum of Nerve Agents and Pesticides

5a. CONTRACT NUMBER
W81XWH-12-2-0047

5b. GRANT NUMBER
W81XWH-12-2-0047

5c. PROGRAM ELEMENT NUMBER

6. AUTHOR(S)
Dr. Dan Tawfik (PhD)
Dr. Joel L. Sussman (PhD)

5d. PROJECT NUMBER

5e. TASK NUMBER

5f. WORK UNIT NUMBER

7. PERFORMING ORGANIZATION NAME(S) AND ADDRESS(ES)
Weizmann Institute of Science, Rehovot 76100 ISRAEL

8. PERFORMING ORGANIZATION REPORT NUMBER

9. SPONSORING / MONITORING AGENCY NAME(S) AND ADDRESS(ES)
US Army Medical Research and Material Command
Fort Detrick, Maryland 71702-5012

10. SPONSOR/MONITOR'S ACRONYM(S)

11. SPONSOR/MONITOR'S REPORT NUMBER(S)

12. DISTRIBUTION / AVAILABILITY STATEMENT
x approved for public release; distribution unlimited

13. SUPPLEMENTARY NOTES

14. ABSTRACT

Project Summary: The long-term objective of this effort is to develop a generic gene shuffling-based technology to rapidly screen libraries of 10^{10} proteins/peptides encoded by DNA libraries, for identifying biomolecules that can intercept both existing and emerging organophosphate-based chemical warfare nerve agents (CWNA). The tasks to be performed at the Weizmann Institute to achieve the major goals of the Center current year are outlined below:
#1. Screening for paraoxon- parathion- malaoxon- malathion- and phorate-hydrolyzing variants.
#2. Validation of the hypothesis concerning the structural motifs in PON1 that are involved in association with HDL, improving rePON1's affinity for HD, and increasing the biological life time of rePON variants.
#3. Steered molecular dynamics. Improvement of the modeling of VX into the rePON1 scaffold, and studies of the mechanism of action of PON1 variants on V-type nerve agents

Relevance: this technology is envisaged to have the capability to facilitate rapid discovery of pre- and post-treatment therapeutic drugs targeted against existing and emerging pesticides and nerve agent threats, and may shorten the time from emergence of a threat to identification of potential counter-measures to a few days or weeks.

15. SUBJECT TERMS Directed evolution, X-ray crystallography, organophosphates, bioscavengers

16. SECURITY CLASSIFICATION OF:			17. LIMITATION OF ABSTRACT	18. NUMBER OF PAGES	19a. NAME OF RESPONSIBLE PERSON
Unclassified			**Unclassified**	36	USAMRMC
					19b. TELEPHONE NUMBER *(include area code)*

Standard Form 298 (Rev. 8-98)
Prescribed by ANSI Std. Z39.18

Table of Contents

Page

Introduction

The long-term objective of this effort is to develop a generic gene shuffling-based technology to rapidly screen DNA libraries encoding mammalian paraoxonase 1 (PON1), and thus to identify variants that can intercept both existing and emerging organophosphate-based chemical warfare nerve agents (CWNA). Enzymes identified in these screens should be capable of catalytically neutralizing the target agent under physiological conditions, thereby providing a basis for development of a new generation of therapeutic agents against CWNA, in either pre- or post-treatment modality. The major milestone is to integrate established components of enhanced molecular evolution techniques so as to provide a means of screening libraries with both greater sensitivity and higher throughput. This effort includes the detoxification of OP-based pesticides

G- and V-type type nerve agents: tabun (GA), sarin (GB), soman (GD), cyclosarin (GF) and VX**,** are highly toxic organophosphates (OPs) that penetrate the body both by inhalation and skin absorption. Commercial OP pesticides such as parathion, chlopyrifos, phorate, and malathion, are also considered as threat chemical agents, especially to civilian populations. In the last 6 years we have used a strategy that utilizes enhanced evolution, protein engineering and 3D structural analysis, together with a specific interception screening protocol, to generate large libraries of mammalian PON1 variants that could be expressed in *E. coli* and screened for their ability to hydrolyse OP nerve agents. Structural analysis was then used to direct the mutagenesis of relevant active-site positions so as to obtain highly effective bioscavengers. The combined approach permitted the isolation of mutants with k_{cat}/K_M values for the detoxification of *in-situ*-generated G agents, such as GD and GF, that approached levels required for them to be considered as efficacious catalytic bioscavenger drugs ($>10^7$ $M^{-1}min^{-1}$). *In vivo* experiments conducted at ICD showed that several variants generated by our group (*e.g.,* 4E9, 2D8, 0C9, and VII-D-11) conferred full protection in pretreated guinea pigs at doses as low as 1 mg/kg protein against $2xLD_{50}$ doses (sc) of GA, GB, GD, and GF. To date, the best variants hydrolyze GD and GF at $3.0\text{-}5.0x10^7$ $M^{-1}min^{-1}$ and GA and GB at ~7-10-fold lower rates. Key variability positions at which changing the residue produces improved hydrolysis of G agents are 69, 115, 134, 136, 222, 291 and 332.

Progress for V agents has been slower than for G agents, due both to the lack of a suitable surrogate molecule that could mimic the methylphosphonyl(*N,N*-dialkylamino ethylthiolate)

moiety of V-type agents, and to the fact that under current screening conditions the starting point, wild-type (wt) rePON1, does not hydrolyze the V-type surrogate, amiton, $[(C_2H_5O)_2P(O)SCH_2CH_2N(C_2H_5)_2]$, at a measurable rate, certainly not at a level detectable in crude bacterial lysates. However, variants in recent libraries (VXR4 and VXR5), screened directly with VX, displayed k_{cat}/K_M values of ~$1x10^5$ $M^{-1}min^{-1}$, and could be used as lead mutants for advanced directed evolution of antidotes against both VX itself and several VX analogs, such as VR.

Body

I. General Aims

The overall specific aims of the project research at the Weizmann Institute are:

1. Development of high-throughput assays for OP hydrolase variants exhibiting high specificity factors and turnover.

2. Provision of proof-of-concept for the proposed core technology employing directed evolution of new recombinant PON and AChE variants.

3. Isolation of interceptors for OP-based commercial pesticides and G- and V-type nerve agents, and expression in soluble form.

4. Large-scale production of selected enzyme candidates, and their kinetic, structural and pharmacological evaluation

6. Establishment of "off-the-shelf" libraries for rapid identification of antidotes against future emerging threats

II. Year 07 specific milestones (of the renewal NIH project):

The tasks to be performed at the Weizmann Institute to achieve the major goals of the Center for the current year are outlined below:

#1. Screening for paraoxon-, parathion-, malaoxon-, malathion-, and phorate-hydrolyzing variants

#2. Validation of the hypothesis concerning the structural motifs in PON1 that are involved in association with HDL, improving rePON1's affinity for HD, and increasing the biological life time of rePON variants

#3. Use of steered molecular dynamics to study the trajectory of interaction of VX with re PON1, improvement of the modeling of VX into the rePON1 scaffold, and studies of the mechanism of action of PON1 variants on V-type nerve agents

#1: Screening for paraoxon-, parathion-, malaoxon-, and phorate-hydrolyzing variants

To obtain a lead for newly designed PON1s capable of hydrolyzing effectively both parathion and paraoxon, we first tested several variants selected from libraries generated towards G- and V-type nerve agents. Evaluation was based on monitoring the release of *p*-nitrophenol.

Results obtained thus far have not revealed a clear trend for parathion. Screening with the oxo metabolite, paraoxon, turned out to be quite successful when libraries VXG6 and VXG7 were searched for mutants with the capacity to hydrolysis it. Results are summarized in Table 1.

Table 1: Catalytic activity towards paraoxon of variants in libraries VXG6 and VXG7 (k_{cat}/K_M, x10^6 $M^{-1}min^{-1}$; figures in parentheses are SD, n=2-4).

Library	Variant	k_{cat}/K_M, paraoxon
VXG6	637C1	5.79±0.10
	610H5	4.44±0.042
	617F7	3.66±0.39
	6bG12	1.23±0.06
	617F4	1.20±0.25
VXG7	114-2-C1	21.2±2.6
	167-mix-A6	2.10±0.30
	268-2-E8	4.69±0.60
	223-1-C3	1.83±0.12
	167-mix-F5	1.65±0.18

As pointed out in our previous (6^{th} year) annual report, sub-libraries of variants of the 6^{th} generation evolved to hydrolyze V agents (VXG6), were constructed based on the 9 most catalytically efficient variants evolved in the 5^{th} round (VXG5) of directed evolution for V-agent hydrolysis. In addition, these were shuffled with oligonucleotides encoding for particular site-specific mutations. Specifically, we targeted residues 72, 189, 192, 193, 196 and 292, which our docking model of VX with PON1 implicated in substrate binding, and especially in leaving-group binding. In addition, we targeted residues 69, 71, 73, 74, 115, 134, 222, 291 and 346. The

7th round PON1 libraries of variants for V-type hydrolysis (VXG7) were generated by targeting mutagenesis to residues that flank both sides of essential active-site residues (E53, W115, N168, M222, N224, D269, S332), which are involved in catalysis and with which the catalytic Ca^{+2} interacts. The underlying rationale was that changes in the closest neighbors of residues essential for catalysis might help to overcome steric, geometric and electronic constraints that reduced catalytic efficiency in the variants generated in the earlier rounds. These permutations were examined vs the OP commercial pesticides.

Regardless of the particular construct, the average proficiency towards paraoxon is 3-10-fold greater than towards VX (the latter being based on the DTNB protocol). The best variant for paraoxon hydrolysis, 114-2-C1, degraded paraoxon approximately 45-fold faster than VX (for VX kinetic data see our 6th Year Annual Report). This variant possesses the I117M mutation, *viz.*, of a residue adjacent to the active-site residue, W115, and in a proximity that may influence the binding and hydrolysis of paraoxon. From the docking model of paraoxon in the active site of PON1, it seems that residue P114 may affect the positions of two catalytically important residues, 69 and 115, and that residue 117 may influence the positions of residues 114 and 115 (Fig. 1).

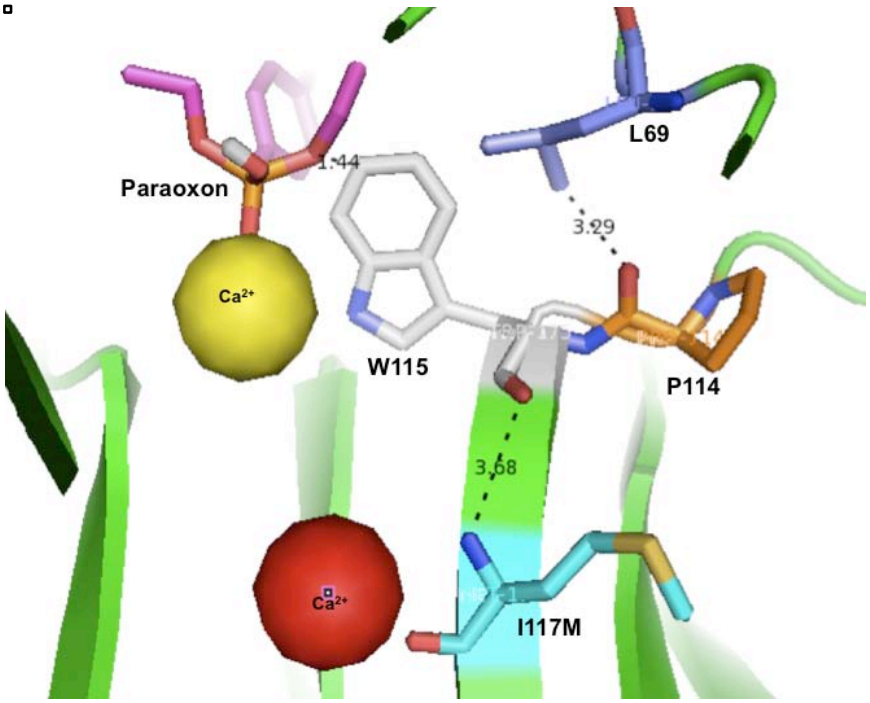

Figure 1. Representation of paraoxon docked within the active site of PON1 that illustrates how W115 and adjacent residues may influence binding of paraoxon and, consequently, its hydrolysis.

These observations call for the reexamination of residues 114 and 117 in the search for an improved catalyst of paraoxon hydrolysis. Specifically, this will involve the generation of libraries that will explore the effects of substitutions at positions 114 and 117 on the efficiency of paraoxon hydrolysis.

To obtain a lead variant capable of effective hydrolysis of malaoxon and phorate, which are defined as threats to the civilian population, we tested the capacity to hydrolyze the two pesticides of the best variants in both the rePON1 and rePTE libraries generated for hydrolysis of G- and V-type nerve agents.

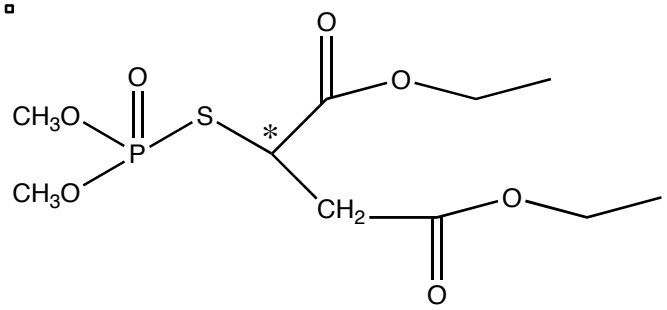

malaoxon

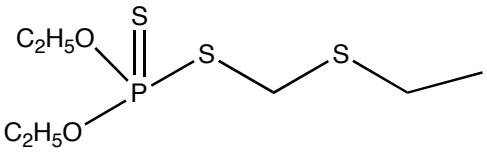

Phorate

Although malaoxon contains an asymmetric carbon atom, the anti-AChE activity of the two enantiomers differs only by 5-7-fold. The data points for the first 30-50% of hydrolysis of malaoxon by rePON1 and PTE variants fitted mono-exponential kinetics very well, and no attempts were made to resolve the individual rates for each enantiomer. Activity on both pesticides was monitored using the DTNB protocol. The exact concentration of each pesticide was determined by monitoring the total release of the corresponding thiol leaving group in the presence of 0.5 M NaF/50 mM phosphate, pH 8.0. Results are summarized in Tables 2 and 3 for rePON and rePTE variants, respectively.

It should be noted that, except for wt PTE and PTE-C23, due to the extremely slow rates of hydrolysis the reactions were recorded up to 30-50% release of the expected amount of the thiol leaving group; thus, if the two enantiomers differ in their rates of degradation by the variants tested, the k_{cat}/K_m values reported for the chiral malaoxon represent the faster isomer.

Table 2: Catalytic activity on malaoxon and phorate of rePON1 variants from libraries VXG6 and VXG7 (k_{cat}/K_m, $x10^3$ $M^{-1}min^{-1}$; single measurements).

Library-Variant		malaoxon	phorate
Wt G3C9		1.0	<1 (no reaction at 2.1 uM over 60 min)
VXG6	10H5	5.1	<2
	7F4	2.0	<2
	bG12	2.5	<2
	7F7	4.5	<2
	7C1	1.7	<2
VXG7	167-F5	8.3	<2
	167-A6	2.4	<2
	223-C3	2.0	<2
	114-C1	6.7	<2
	268-E8	4.6	<2

Table 3: Catalytic activity on malaoxon and phorate of PTE variants (k_{cat}/K_m, $x10^3$ $M^{-1}min^{-1}$; single measurements).

Library-Variant		malaoxon	phorate
Wt S5		29 and 14 (two different preps)	19.5
Early libraries	I19	1.1	
	C74	2.1	2.5
	A57	8.1	
	E36	3.4	3.3
Library G5	C23	14	14; 21
	A53	8.2	6.2
Library G6	IID9	1.8	2.0
	VF9	4.9	4.8
	IF4	1.6	4.6
	IIID10	3.2	4.4
	IVH3	2.0	5.5
	VA4	2.6	5.6

All the rePONs tested displayed very poor activity, if any, towards phorate. Under the experimental conditions employed, with an enzyme protein concentration of 0.5-2 mM in the assay cuvette, the activity measured was indistinguishable from the rate of spontaneous hydrolysis of the combined DTNB/phorate blank cuvette (0.0024 min^{-1}). Thus, we estimated k_{cat}/K_M for all the rePONs listed in Table 2 to be $<2x10^3$ $M^{-1}min^{-1}$. Phorate is probably a poor substrate for PON1 due to its especially unfavorable structure, which contains both P=S and P-S-alkyl moieties (combining both thiono and thiolo barriers). In the case of malaoxon, the rate of spontaneous hydrolysis of DTNB/malaoxon was 0.0028 min^{-1}, viz., only 2-3-fold slower than hydrolysis in the presence of ~1 μM rePON1, thus highlighting the fact that the advanced rePON1s variants tested have evolved specifically to accommodate the $CH_3P(O)O$-alkyl- moiety of VX, and are less suitable for binding dialkyl-based OPs such as malaoxon and phorate.

As expected from the catalytic advantage of bacterial PTEs over rePONs when reacting with paraoxon or parathion, the PTE variants were more active than the rePONs towards both phorate and malaoxon. However, the observed values for k_{cat}/K_m listed in Table 3 indicate that the variations introduced into the PTE scaffold so as to accelerate the hydrolysis of V-agents, did not allow for sufficient catalytic activity on either phorate or malaoxon to permit their consideration as antidote candidates for either of these OPS. In fact, with the exception of C23, in all cases the mutations introduced decreased catalytic activity relative to the wt enzyme. It should be noted that, despite the potent catalysis of paraoxon and parathion (both diethyl phosphate-based pesticides) by the wt PTE variant S5, its activity towards the dimethylphosphoryl analog is reduced significantly, presumably due to lack of tight binding relative to the diethylphosphoryl homolog. Thus, we found that parathion (containing diethoxyphosphoryl) is hydrolyzed by wt S5 20-fold faster than its dimethoxy homolog, methyl parathion; this despite the greater electron donating properties of the ethoxy relative to the methoxy group, which should decrease the electropositivity of the P atom, thus making it an inferior substrate to methyl parathion. Indeed, fluoride was found to hydrolyze parathion 3-fold more slowly than methyl parathion. Thus, the low k_{cat}/K_m values observed for hydrolysis of malaoxon by the PTEs are attributed to the combined effects of poor molecular complementarity of the malaoxon molecule and of the thiolo barrier.

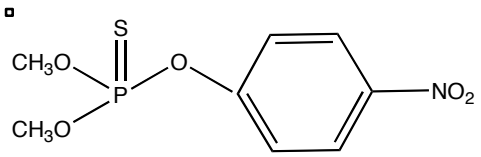

Methyl parathion

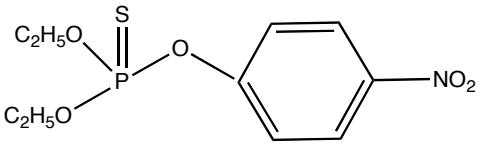

parathion

As expected, the conversion of the P=O of malaoxon to the thiono function (P=S) of malathion further decreased the susceptibility of this OP type to both rePTEs and rePONs.

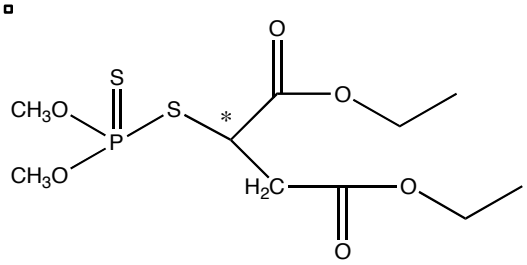

malathion

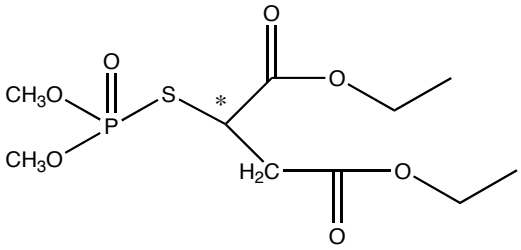

malaoxon

Thus, when PTE variants of library 6 (IID9, VF9, IF4, IIID10, IVH3, and VA4, at 0.4-1.0 μM) were reacted with malathion, the activity measured was indistinguishable from the spontaneous rate of chromophore release in the combined DTNB/malathion control run (0.0015 min^{-1}); we therefore estimate that k_{cat}/K_m of these variants is $<2x10^3$ $M^{-1}min^{-1}$. The five best rePON1 variants of library VXG7 (114-C1, 167-A6, 167-F5, 223-C3, and 268-E8) also did not display a measurable increased activity over control values towards malathion, despite the fact that they were at 1.5-3 μM in the final reaction mixture. We conclude that the dimethoxy phosphoryl pesticides are very poor substrates of the OP hydrolases examined, and that a different line of study is required to evolve variants with sufficient activity to qualify as bioscavengers of the dimethylphosphoryl-based OPs.

#2. Validation of the hypothesis concerning the structural motifs in PON1 that are involved in association with HDL, improving rePON1's affinity for HD, and increasing the biological life time of rePON variants

In order to increase the stability of rePON1 variants in the circulation we examined the influence of the known capacity of PON1 to interact with HDL, which is accompanied by an

increase in its catalytic activity. We earlier hypothesized that the H2 helix and its connecting loops, the H1 helix, and the flexible loop residues, are together responsible for the structural changes that result in stimulation of activity when PON1 is bound to HDL (see our 2nd Annual Report).

In order to test the importance of individual residues on HDL binding we developed a cell-free system that permits the synthesis of rePON1 and its various mutants in the presence of HDL (depicted in the cartoon below). The advantage of this technique is that it alleviates both the need for protein purification in detergent buffers, and for subsequent removal of detergent prior to testing the interaction of variants with HDL. Indeed, removal of detergent from purified rePON1 was found to greatly compromise its stability. In addition, this assay system can be used to analyze many mutants in parallel. The selection of putative key positions in PON1's helices was based on structural analysis of our rePON1 crystal structures, as well as on sequence analysis of the PON family.

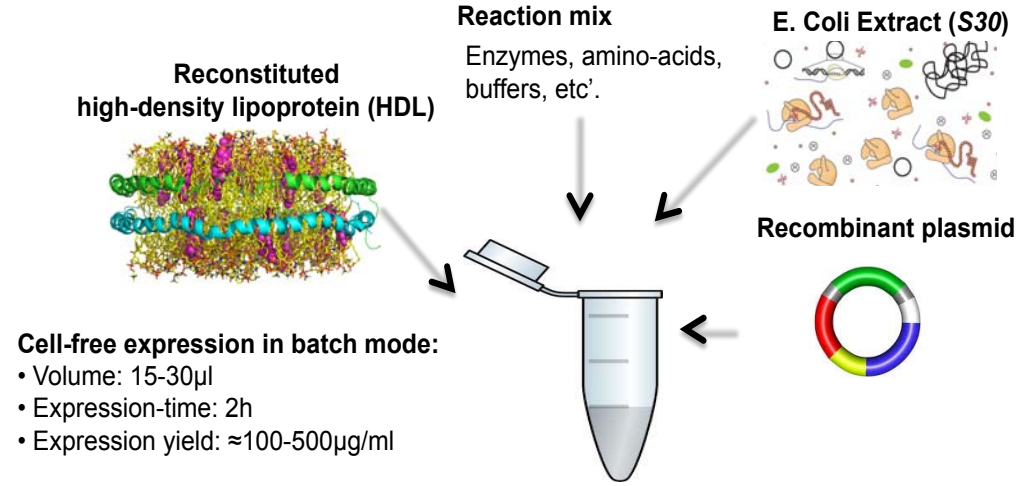

In our 6th year Annual Report we summarized the preliminary data that pointed to the involvement of Y185 and F186, within the H2 connecting loop, especially of F186, which displays a significant decrease in the stimulation of activity towards TBBL. We also pointed out that residue Y71, within the flexible loop, which moves significantly upon binding of 2HQ, is likely to be a key residue in stimulation of the lipo-lactonase activity of rePON1. Furthermore, unlike the L198Y mutation, which results in both stabilization and stimulation of activity by this H2 residue, the L198W mutation results only in stimulation of activity relative to the WT.

We report here on the evaluation of positions in the H1 helix and in the active-site region of the wt G3C9 variant, for which results are summarized in Table 4.

Table 4: Mutations in helix H1 and within the active site produce enhanced stability and activity relative to WT rePON1 in the presence of HDL

Variant	Activity stimulation		Inactivation 144hr
	K_{app}(μM)	V_{max} (%)	Residual lactonase activity (%)
rePON1	0.58±0.07	406±11	61±6
A6V	0.53±0.07	505±15	84±3
L7V	1.3±0.17	364±13	42±5
T8V	0.41±0.05	508±11	73±7
T8I	0.44±0.01	450±3	66±4
G13V	0.58±0.05	500±12	74±5
Y71F	0.38±0.1	467±14	41±4
Y71G	1.70±0.09	430±7	35±6
H184Q	1.5±0.2	367±12	6±2
H184T	1.00±0.09	613±14	84±3

The first row entries, for rePON1, are relative to the same amount of protein in the absence of HDL. Activity stimulation refers to TBBL hydrolysis, and inactivation tests were performed in the presence of 15 mM EDTA at 37^{o}C. Residues 6, 7, 8 and 13 are on the H1 helix, and 71 and 184 are located within the active site.

As can be seen, stimulation of activity for wt rePON1 in the presence of HDL was ~4-fold. Mutations at positions 6 and 13 of H1, and at active-site residue 184, further increased activity. This enhancement was accompanied by increased stability for mutations at positions 6, 13 and 184.

Thus far, our conclusions were based on the stabilization and enhanced activity revealed by monitoring lactonase activity. To demonstrate the broad-spectrum enhancement achieved by association with HDL, the activity of several variants obtained by mutating the G3C9 scaffold was monitored towards the VX surrogate, EMP, in which the diisopropylamino-ethanthiolo leaving group had been replaced by coumarin. As shown in Fig. 2, increasing the HDL concentration produced complexes of both the G13V and H184T mutants that displayed

increased activity relative to the wt enzyme. Deletion of the 20 amino acids at the N-terminus decreased activity, and thus substantiated the importance of this region in binding to HDL

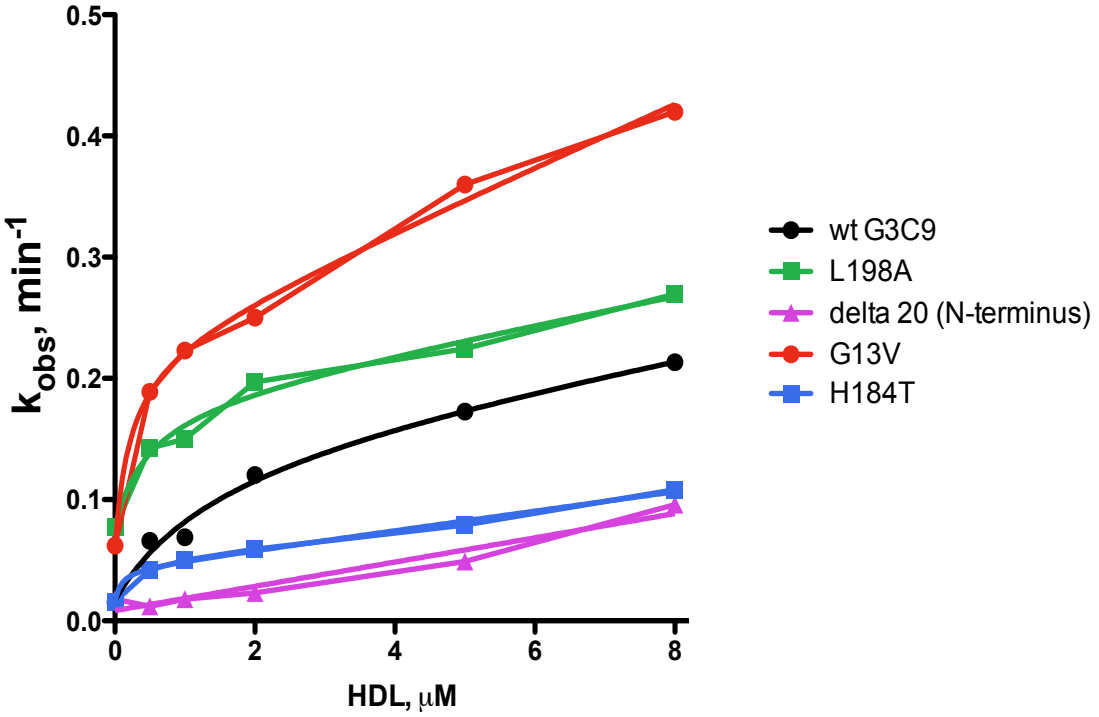

Figure 2: Increased binding of PON1 to HDL increases its catalytic activity on the VX surrogate, EMP.

When the best mutated positions in wt G3C9 were copied onto the IIG1 scaffold (which is the most effective variant towards cyclosarin and soman), and tested on the cyclosarin surrogate, CMP, we obtained essentially the same pattern of enhancement, albeit with a reduced efficacy compared to the wt G3C9 (see Fig. 3 below). Thus, the effects of modification of the H1 and H2 helices, together with the connecting loops, are dependent on other residues yet to be identified.

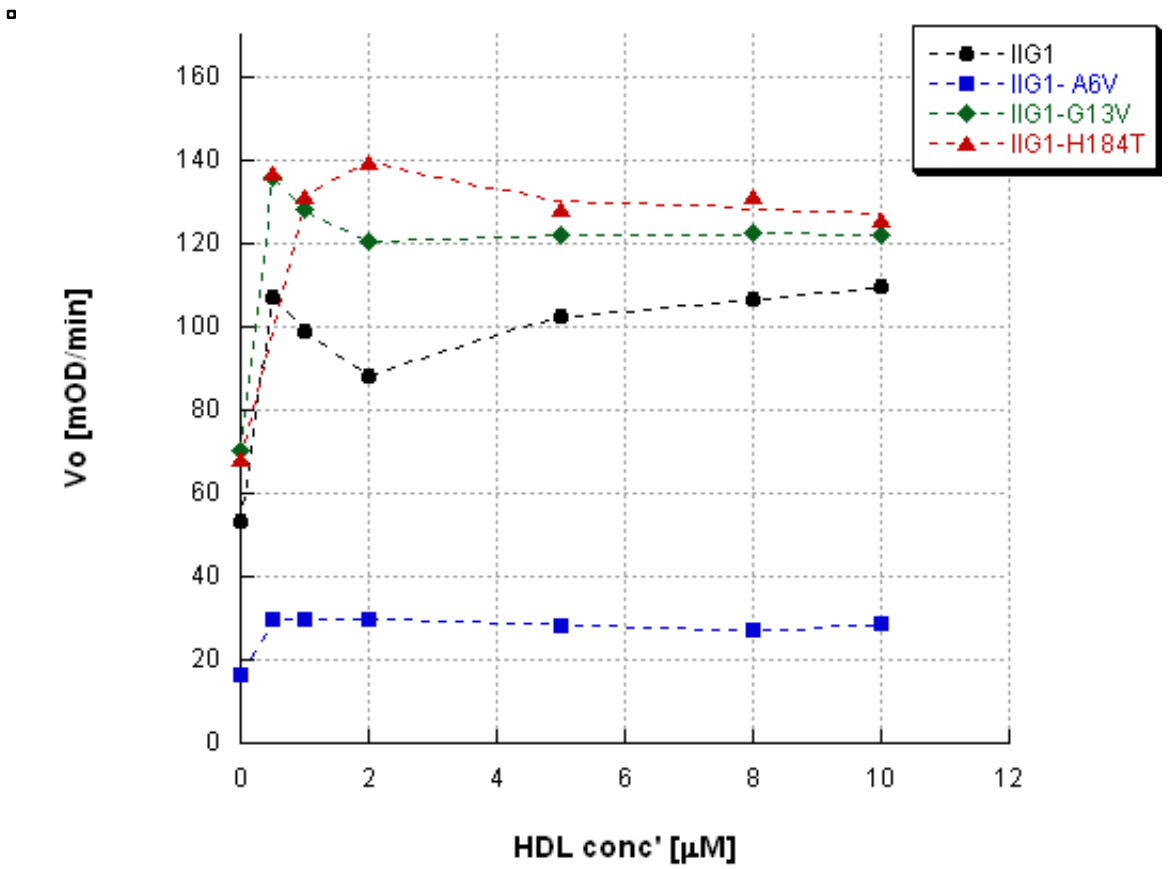

Figure 3: Stimulation of hydrolysis of the GF analog CMP due to binding to HDL

In order to examine whether mutations that can stimulate rePON1 activity and enhance its stability *in-vitro* can also provide it with an increased circulatory half-life *in-vivo*, we sent the following variants for large-scale production and purification by the Magliery lab at OSU, to be followed by *in-vivo* pharmacokinetics testing by the Cerasoli lab at ICD: A6V-G3C9 and G13V-G3C9, variants that display increased HDL binding, and Del20-G3C9, a variant that displays decreased HDL binding relative to G3C9, and thus provides a negative control. By comparing the *in-vivo* circulatory half-life times of these proteins relative to wt-rePON1 (G3C9), we should be able to validate our hypothesis, and provide an approach to enhancing the pharmacokinetic properties of rePON1 variants.

On August 26th, 2013, all three rePON1 clones (A6V-G3C9, G13V-G3C9 and N-Del20-G3C9) were sent to OSU for expression and purification, with the aim of studying their PK profile in guinea pigs at ICD. We are awaiting the results of the *in vivo* experiments so as to design the next generation of variants with increased affinity for HDL.

In the appendix we summarize a comprehensive study that describes the structural and mechanistic basis for the HDL-induced stimulation of PON1's activity.

#3. Improved modeling of VX within the rePON1 scaffold

The objective of this modification was to enhance the accuracy of Steered Molecular Dynamics (**SMD)** and Molecular Dynamics (MD) simulations for docking of VX, in order to achieve improved prediction of the properties of newly designed rePON1 mutants. Fig. 14 models the complex of 1-6-G4 (from round VXG4) with the toxic S_p-VX enantiomer. This variant is ~100-fold more active toward VX than the wt enzyme. The mutations in the variant were copied into the G2E6 crystal structure, with the exception of two residues that are not within the active site:

- 1-6-G4: L55I, L69V, K70N, Y71M, H115W, H134R, H184A, K192Q, F222M, T332S

The model was generated with a new simulation approach, and the most important differences from our previous modeling are as follows:

1) The protein and ligand were parameterized by using Amber99sb-ildn force field [1] rather than the OPLS/AA force field [2,3] that was used previously. It has been shown that simulations of proteins parameterized with the Amber99sb-ildn force field reproduce results of NMR studies better than any other modern force field [4].

2) Another advantage of the Amber99sb-ildn force field is the possibility of introducing a more sophisticated model of water - TIP5P [5], which is not possible with OPLS/AA. TIP5P reproduces the electrostatic properties of water better than the previously used TIP4P [6]. In TIP5P, lone electron pairs on the water oxygen are represented by pseudo-atoms. This permits improved accuracy of simulations of biomolecular interaction phenomena in which microscopic behavior of water molecules plays an important role, as is the case in PON1-mediated catalytic OP degradation (Fig. 1).

3) A new simulating pipeline was deployed on a fast GPU device, which increased the speed of simulation significantly.

It is envisaged that the overall increase in the reliability of the simulation methodology will improve the accuracy of the prediction of the catalytic properties of new, rationally designed variants of rePON1s when reacting with V-type nerve agents. Compared to previous attempts, the current results generate a more detailed description of the initiation of the catalytic process and provide better input for further study, for example with QM/MM methods.

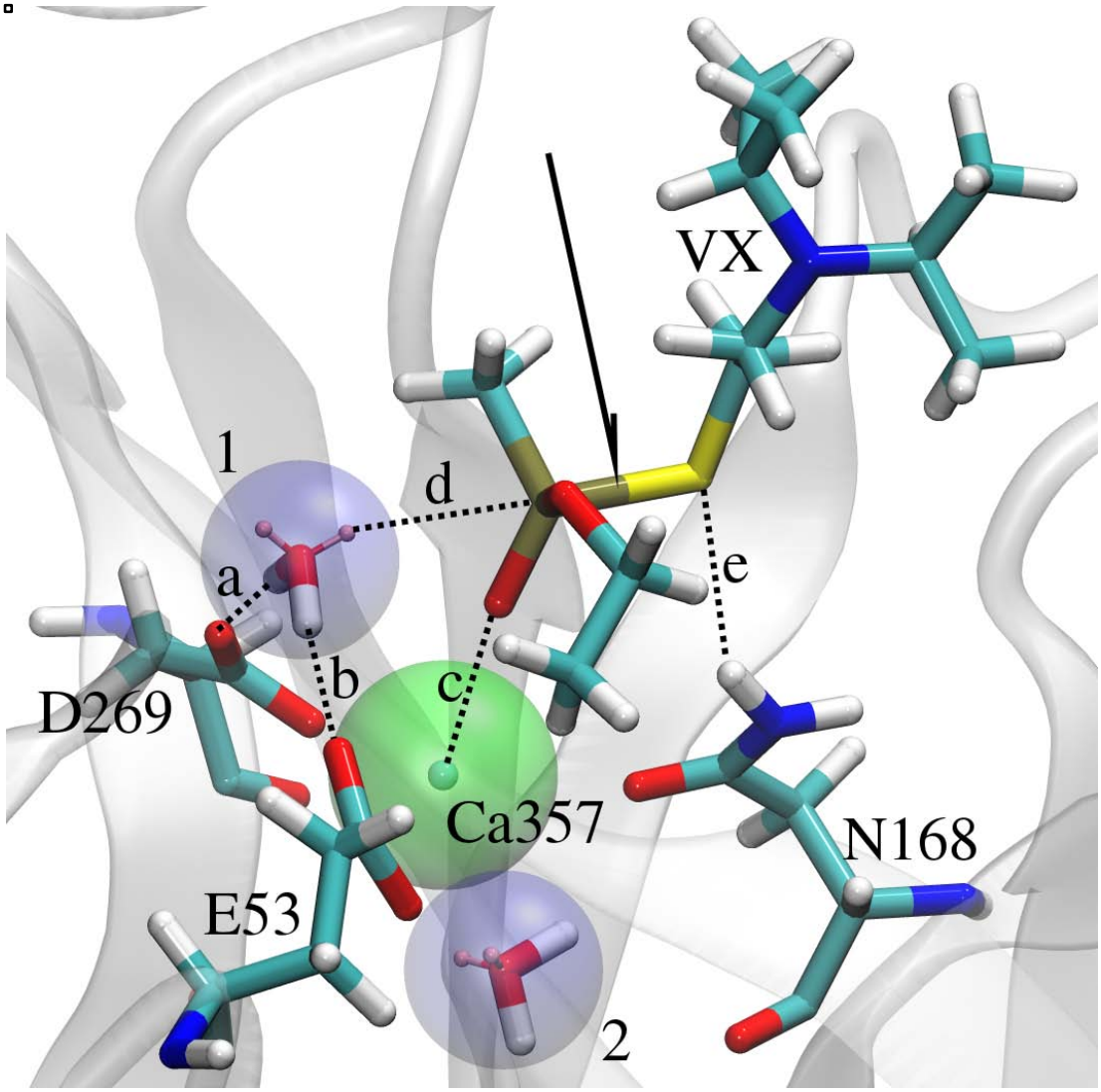

Figure 14: Model of the 1-6-G4 rePON1 variant complexed with Sp-VX.

The orientation of VX fulfills the criteria of the binding mode necessary for catalytic breakdown of OP according to the mechanism that is considered the most probable [7]. In this mechanism, a hydroxyl ion produced by deprotonation of water "1" by D269 and E53 (lines "a" and "b") attacks the phosphorus atom of VX (electrostatically attracted to the catalytic calcium

ion, Ca357 - line "c") along the line "d". As a consequence, the S-P bond, marked by the arrow, is severed. The leaving group is stabilized by a possible H-bond with N168. Structural water "2" is conserved in all the rePON1 crystal structures. It is proposed that this water molecule mediates transfer of the proton of the carboxyl group of residue E53, and restores its structure in the native enzyme so as to initiate a new catalytic cycle.

Key Research Accomplishments

- Identification of a variant catalyzing hydrolysis of paraoxon at $2x10^7$ $M^{-1}min^{-1}$
- Elucidation of the structural and mechanistic basis for the HDL-induced stimulation of PON1's lactonase activity. Improved capacity to associate rePON1s with HDL,
- Use of steered molecular dynamics (SMD) methodology to model the interaction of VX with PON1

Conclusions

- Screening existing libraries with paraoxon, parathion, malaoxon, malathion, and phorate showed that with the exception of paraoxon, all the rePONs tested displayed poor activity, if any, and a different line of enhanced evolution will have to performed so as to generate variants capable of hydrolyzing them effectively.
- The improved modeling of VX into rePON1, so as to achieve enhanced proficiency in the design of new variants suggests several sites for introducing mutations that will enhance rates of degradation of V-type nerve agents.
- The comprehensive study of rePON1-HDL association identified residues involved in both enhancement of catalysis, as well as residues that produced enhanced thermal stability, offering new approaches to extension of the biological life-time of rePONs.

References

[1] Lindorff-Larsen K. et al. Proteins 2010, **78**(8), 1950-1958.
[2] Jorgensen WL, Tirado-Rives J. *J. Am. Chem. Soc*. 1988, **110**(6), 1657-1666.
[3] Jorgensen WL, Maxwell DS, Tirado-Rives J. *J. Am. Chem. Soc*. 1996, **118**(45), 11225-11236.
[4] Beauchamp, KA *et al*. *J. Comp. Theory Comput*. 2012, **8**, 1409-1414.
[5] Mahoney MW, Jorgensen WL. *J. Chem. Phys*. 2001, **114**, 363-366.
[6] Jorgensen WL *et al*. *J. Chem. Phys*. 1983, **79**, 926-935.
[7] Ben-David M *et al*. *J. Mol. Biol*. 2013, **425**(6), 1028-1038.

Appendix-Supplementary

Model for the binding of PON1 to HDL

In this appendix we provide a detailed description of a model for the binding of PON1 to HDL, especially with regard to the H2 residues, obtained via mutational and structural analyses of PON1 along with computational simulations. We thus describe the structural and mechanistic basis for the HDL-induced stimulation of PON1's lactonase activity. Furthermore, we discuss this model within the framework of a more general hypothesis regarding the importance of structural rigidity, and the importance of second- and third-shell residues, in configuring enzyme active sites.

The PON1/HDL structural model

We already earlier postulated the interactions of PON1's helices H1 and H2 with the surface of HDL, based primarily on the presence of exposed, surface hydrophobic residues, especially of aromatic amino acids (Gaidukov & Tawfik, 2005; Harel et al, 2004) (**Figure S1**). However, the proposed model did not address the key question – namely, how does HDL binding induce dramatically higher stability and catalytic efficiency. Our working hypothesis has been that HDL binding would immobilize the PON1 segments attached to it, which, in turn, would affect the active-site's shape and/or catalytic organization. In this context, we have now examined the B-factors of available PON1 structures, and found that the C-terminal end of H1 (the N-terminus is completely disordered) and H2 comprise the most mobile parts of the enzyme. In accordance, the normal mode analysis of these structures (NMA; ElNemo server - http://igs-server.cnrs-mrs.fr/elnemo/) revealed that helices H1 and H2 show large, coordinated motions. This motion results in very different configurations of the active site's opening, and in the displacement of catalytic residues, most notably N168 (a Ca^{+2}-ligating residue) and the catalytic Ca^{+2} (**Figure S2A-B**).

Further analysis of the crystal structures of rePON1s in the region of helices H1 and H2 revealed potential interactions of a molecule of the detergent *n*-dodecyl-beta-*D*-maltoside (DDM) that was present in the crystallization medium. The detergent seems to interact with residues of H1 (*e.g.*, Q20), as well as with the adjacent H2's N-terminal connecting loop (L200 and W202; **Figure S2C**). The detergent, and presumably the lipid components of HDL, may thus

restrict these H1-H2 motions. Indeed, the packing surfaces between rePON1 molecules within the different asymmetric units of the unit cell involve close interactions between the adjacent H2 helices, as well as between their connecting loops, and specifically between residues Y185 and F186 of the neighboring PON1 molecules (**Figure S2D**). It appears, therefore, that both the bound DDM molecules, and the crystal packing interactions involving H1 and H2, play a major role in limiting PON1's conformational flexibility and, appear to affect the way crystals form. Given the hydrophobic nature of these interactions, they are likely to mimic the binding interactions of PON1 with HDL. Furthermore, the H1 and H2 configurations seen in the crystal structure may represent only one out of many possible configurations available for these helices, and hence of PON1's active-site. Since conformational flexibility promotes instability and faster unfolding rates (Matthews et al, 1987), HDL binding increases the enzyme's thermodynamic stability (as does detergent binding, though to a lesser degree). Similarly, the preferred adoption of a specific active-site configuration may account for the HDL-induced increase in catalytic efficiency.

***In situ* incorporation of rePON1 into reconstituted HDL particles**

The experimental protocol applied thus far for the analysis of PON1's interaction with HDL includes: 1) production and/or purification of recombinant or of human PON1 in the presence of a detergent; 2) delipidation for removal of the detergent; 3) incubation of the detergent-depleted PON1 with HDL. Aside from being laborious, this protocol is problematic due to the rapid inactivation of the delipidated PON1. Thus, the observed catalytic stimulation might be over-estimated when compared to a partly inactive control devoid of lipids. To enable faster and more reliable analysis, we developed a cell-free expression system that permits the expression of rePON1 in the presence of reconstituted HDL particles (rHDL). The latter were prepared as discoidal rHDL particles containing 1-palmitoyl-2-oleoylphosphatidylcholine (POPC), free cholesterol (FC), and the apolipoprotein apoA-I, at a molar ratio of 100/5/1 (Gaidukov et al, 2010; Oda et al, 2001). We first validated the reliability of this procedure by testing the stimulation of activity of the wt-like rePON1 towards a chromogenic lactone substrate, TBBL, and towards paraoxon. We measured the activity of the cell-free expression products at 0-10 μM rHDL.

The results obtained with this novel procedure were in agreement with those obtained with the previously applied delipidation protocol (Gaidukov & Tawfik, 2005; Gaidukov et al, 2010). In essence, PON1-catalyzed TBBL hydrolysis was stimulated by HDL, following a typical Langmuir isotherm, and the V_{max} values (percentage activity relative to the activity of the cell-free translated PON1 in the absence of rHDL) and K_{app} (the rHDL concentration that produces 50% of the total stimulation of activity) displayed similar trends. As previously observed, the paraoxonase activity showed only minor stimulation, and stimulation of lactonase activity was completely abolished in the H1-truncated form.

The effect of rHDL on the stability of rePON1 was explored by a previously applied inactivation assay. The cell-free expressed PON1 samples in the absence of HDL, and at the highest rHDL concentration (10μM), were incubated at 37°C in the presence of a calcium chelator, EDTA. The residual lactonase activity was tested after incubation with EDTA for 72 h, and compared to the activity prior to EDTA addition (**Table S1**). The decreased inactivation rates upon HDL binding (Gaidukov & Tawfik, 2005; Gaidukov et al, 2010) were similarly reproduced. **Table S1** reveals that lactonase stimulation and stabilization are overall correlated.

Mutational analysis of H2 and of its C-terminal loop

Truncation of H1 resulted in a ~100-fold drop in affinity for HDL, and in abolition of both HDL-mediated stabilization and stimulation of enzymic activity, thus providing evidence for the role of H1 in the HDL binding (Gaidukov & Tawfik, 2005) (**Table S1**). Since complete truncation of H2 is not an option, point mutations were explored with the aim of examining the role of H2 in HDL binding.

H2 and its C-terminus loop possess a stretch of hydrophobic surface side-chains that were postulated to be involved in the binding to HDL (Gaidukov & Tawfik, 2005; Harel et al, 2004). These include H2 residues Y190, W194 and L198, and the C-terminal loop residues Y185 and F186 (**Figure S1**). The mammalian PONs exhibit high sequence conservation at these positions – a degree of conservation that is unexpected for surface residues. Some positions are fully conserved (*e.g.,* positions 183-186), and others display only conservative substitutions (*e.g.,* position 190, Tyr vs. Phe). Following the structural and sequence analyses, we designed mutants that sample H2 residues Y190, W194 and L198, as well as Y185 and F186 within H2's C-terminal loop (**Figure S1**). Substitutions to Ala, especially of positions 190 and 194, reduced the

HDL-induced stabilization and lactonase stimulation (**Table 1**), with the 190/194 double mutant showing almost no stimulation or stabilization (V_{max}/K_{app} values reduced by ~14-fold). Mutations in H2's N-terminal loop also had a marked effect. While Y185A showed comparable parameters to that of the wild type, Y185G, that is likely to induce changes not only in the side-chain, but also in the loop's backbone configuration, resulted in near-complete loss of the effects of HDL. Both F186A and F186G resulted in a decrease in lactonase stimulation and stability (**Table S1**). The double mutant, Y185A/F186A, showed a >10-fold decrease in both lactonase stimulation and stability (**Table S1**). Overall, these results support the hypothesis that residues of helix H2, as well as of its connecting loop, play a role in HDL binding.

The mechanism of PON1's catalytic stimulation

PON1's crystal structures reveal a long loop that connects the N-terminus of H2 with the enzyme's scaffold and active site. This loop also includes the active-site residues H184 and D183 (**Figures S2B and S3**). Mutations in these two residues render both human PON1 and rePON1 almost inactive (Josse et al, 1999; Khersonsky & Tawfik, 2006). However, a detailed analysis indicated that neither of these residues is directly involved in catalysis, *i.e.*, as a base or acid catalyst (Khersonsky & Tawfik, 2006). Indeed, analysis of the crystal structure of the wild-type-like rePON1 in complex with a lactone analogue revealed no direct contacts of the substrate with either D183 or H184, and hence the proposed catalytic mechanism did not include these residues (Ben-David et al, 2012). These residues, especially D183, are highly conserved, and are found in very distant members of the PON family (*e.g.*, bacterial PONs with <30% sequence similarity to mammalian PONs) (Bar-Rogovsky et al, 2013). What then are the roles of H184 and D183?

Despite the absence of direct contacts, there exists a network of hydrogen bonds spanning from H2's C-terminus loop, and particularly residues H184 and D183, to two active-site residues that are in direct contact with the substrate: residue Y71 – at the tip of a highly mobile active-site loop (residues 70-81), and the catalytic Ca^{+2}-ligating residue, N168 (**Figure 3S**). As shown (Ben-David et al, 2012; Ben-David et al, 2013), conformational variations in the mobile active-site loop, as well as in the catalytic Ca^{+2}, modulate rePON1's catalytic activity, and specifically relate to the enzyme's dual activity as a lactonase (the native function) and as a paraoxonase (a

promiscuous activity). We thus reasoned that the lactonase stimulation seen upon HDL binding might be mediated via the hydrogen bonds of D183 to Y71 and/or to N168 (**Figure S3**).

To examine these two options, we prepared a set of mutants in residues that are part of the network that includes D183-H184, Y71 and N168 (**Figure S3**). As previously reported, all mutations at positions 183 and 168 resulted in complete loss of both the lactonase and paraoxonase activities. Other mutants did show detectable activity, including Y71F, Y71G, H184Q and H184T. These mutations had a relatively mild effect on the lactonase activity (<6-fold decrease towards TBBL (Khersonsky & Tawfik, 2006)). We thus tested the HDL-induced stimulation of the activity of these mutants. The conservative Y71F, but also the drastic Y71G mutation, resulted in only a mild decrease in the HDL-induced stabilization and catalytic stimulation (<3-fold; **Table S1**). Foremost, abolishing the putative H-bond between Y71's hydroxyl (via the Y71F mutation) and D183 (**Figure 3**) had no effect on the HDL-induced stimulation of activity (**Table S1**). This suggests that the putative hydrogen bonds of 183D-184H with Y71 do not play a key role in PON1's activity in general, and specifically in the HDL-induced stimulation.

The hydrogen bonds spanning from H2, including K192, to N168, are much more likely to be crucial for catalysis. This hypothesis is supported by the absolute essentiality of N168 (mutants of other residues that ligate the Ca^{+2} - 53, 224, 269 and 270 - do display some residual activity) (Ben-David et al, 2013)) and of D183 (Khersonsky & Tawfik, 2006), and by the known effects of the 192Q/R polymorphism on HDL binding and stimulation of activity.

The role of H184 in aligning D183, and in turn N168, is supported by the fact that mutations of H184 to non-polar residues, *e.g.,* to Ala (Josse et al, 1999; Khersonsky & Tawfik, 2006), result in loss of activity, but polar residues such as glutamine or threonine retain activity and stimulation, or even slightly increase the stimulatory effect of HDL (H184T; **Table S1**). Further, PON1's denaturation is initiated by the loss of the catalytic Ca^{+2}, followed by loss of the structural one, and irreversible unfolding (Gaidukov & Tawfik, 2005; Kuo & La Du, 1998). The spatial fixation of N168 by D183, and the accompanying electrostatic effects that may stabilize the catalytic Ca^{+2}, make a significant contribution to the affinity of the catalytic Ca^{+2} for PON1. Thus, limiting the conformational freedom at the H1-H2 interface (**Figure S2**), and thereby reinforcing the H-bond network that immobilizes N168 and, in turn, the catalytic Ca^{+2} (**Figure**

S3), provides a likely explanation for the effects of HDL-binding on both PON1's lactonase activity and its configurational stability.

EVB simulations

A crystal structure of PON1 bound to an HDL particle, or for that matter, of any other HDL-associated enzyme, is unavailable. Thus, the structural changes induced by HDL binding, and their effect on the active-site configuration, remain unknown. To gain further insights regarding the mode of stimulation of PON1 activity, we therefore used the crystal structure of the wild-type-like rePON1 as the basis for empirical valence bond (**EVB**) simulations. Our working assumption has been that the changes in PON1's lactonase activity upon HDL binding relate primarily to the conformation of H2, as indicated by the experimental data presented above. A series of EBV models were generated by: (1) simulating the gradual pulling of H2 away from the active site; (2) using a range of H2 configurations obtained from normal mode simulations (**Figure S1A**, **B**). Simulations were performed in the presence of a lactone substrate (TBBL) that represents PON1's lipophilic lactone substrates, as well as with paraoxon, a promiscuous substrate. The models were simulated and relaxed for 100 ps at 300K.

Two alternative models for the TBBL/PON1 complex were examined. Both models were based on H115 as the general base generating the hydroxide nucleophile (Ben-David et al, 2012). The models differed by either N168 or H285 providing leaving group assistance (LGA), and the substrate's orientation was refined accordingly. We found that during relaxation, the structures with either no perturbation or minor perturbation of H2's position maintained well-ordered active sites. Specifically, N168 and N224 maintained a close interaction with the both the metal ion and the substrate. However, upon more significant perturbation of H2, the side-chain positions of both H184 and D183 were disturbed, and subsequently, the catalytic Ca^{+2}'s interaction with N168 was severely altered (**Figure S4**). Simulations were also performed with H2 constrained throughout the relaxation step and EBV runs. This might suggest that H285 only serves as an auxiliary, backup residue (Ben-David et al, 2012) in cases in which N168 is highly fluctuating (*i.e.*, when PON1 is not bound to HDL).

EVB models with paraoxon were also examined, with D269 as the general base (Ben-David et al, 2013). As seen with the TBBL models, perturbing the position of H2 affected the network of interactions that includes H184, D183 and N168. Nonetheless, the active site maintained its

catalytic configuration for paraoxon hydrolysis. Notably, N224's side-chain showed some flexibility, whereas, as opposed to the lactone hydrolysis trajectories, N168 largely remained fixed. The fixation of N168 despite H2's conformational freedom seems to be driven by the interaction of N168 with paraoxon's well-positioned leaving group oxygen. Thus, paraoxon hydrolysis seems to be less sensitive to the active site's configurational ensemble, which is in line with paraoxon being a promiscuous substrate, and with HDL binding inducing a minor change in PON1's paraoxonase activity - ~1.5-fold stimulation, as compared to ≤20-fold towards lactones (Gaidukov & Tawfik, 2005).

Crystal structure of the 192Q mutant

The 192R/Q variants are polymorphs of human PON1 that were reported to differ in their antiatherogenic potential, with the 192R isozyme displaying higher potency (Costa et al, 2013; She et al, 2012). It was accordingly found that the 192Q polymorph exhibits significantly reduced HDL binding and lactonase stimulation. Similarly to rabbit PON1, rePON1 has Lys at position 192. RePON1-192K and -192R show essentially the same level of stability and activation upon the association to HDL, whereas, similarly to the human polymorph, re-PON1-192Q shows reduced stability and stimulation (Gaidukov et al, 2006). However, the structural basis for the different behavior of 192K/R versus 192Q remained thus far unexplained.

Previously solved crystal structures of rePON1-192K indicate that K192 resides on H2, with the side-chain pointing towards the active site (**Figure S3**; PDB codes: XXXX). We have now determined the crystal structure of re-PON1-192Q. As in our previous studies, rePON1 variant G2E6 was used for crystallization. Crystals of rePON1-192Q diffracting to 2.3Å were obtained as for G2E6 (192K) (Ben-David et al, 2012; Ben-David et al, 2013), in the same space group and with very similar unit cell parameters (**Table S2**).

Superimposition of rePON1-192K (PDB code: 3SRE) and the rePON1-192Q mutant structures reveals no major changes in backbone or side-chain orientations (**Figure S5A**). However, the presumed hydrogen-bonding network that connects H2 to N168 differs. The amide group of Q192 is in close contact with the backbone carbonyl of F186 (2.9Å, *versus* 4.8Å to the e-amino group of 192K), and the distance to the side chain of S166 becomes shorter (2.6Å vs. 3.1Å in 192K; **Figure S5**). F186 seems to be involved in HDL binding, and perturbations of the loop's backbone at this residue seem to have a marked effect as indicated by the F186G mutation

(**Table S1**). It thus likely that the K192Q mutation stabilizes the C-terminus connecting loop in an unfavorable configuration, such that the HDL binding effects on H2 are markedly reduced.

Interim Conclusions

The mutational and structural analyses presented here provide the first clear evidence for the involvement of helix H2 and its C-terminal loop in the binding of PON1 to HDL, and in the stabilization and stimulation of catalytic activity that ensue. The residues that show the most pronounced effects appear to be Y185 and F186, which reside on the C-terminal loop, and Y190 and W194, which reside on H2 itself (**Table S1**). Thus, our refined model for the binding of PON1 to HDL includes three sets of interactions: the N-terminal membrane-anchoring helix H1, helix H2, and H2's C-terminal connecting loop (**Figure S1**). The high configurational flexibility of helices H1 and H2 is likely to be reduced significantly by HDL binding, thus accounting for the dramatic stabilization of PON1's overall configuration, and specifically of its active site and catalytic Ca^{+2}.

At the technical level, the cell-free expression of PON1 in the presence of reconstituted HDL particles offers a new approach to study the interactions of other enzymes, or proteins, with HDL, or with lipoprotein particles in general. This method is relatively fast and, foremost, allows production of stable membrane-associated enzymes without the introduction of detergents.

The mechanism of catalytic stimulation of PON1 unraveled here seems to involve a complex network of interactions that spans from H2, and especially its C-terminal loop (residues 183-187), into the active site. This network includes two key active-site residues, D183 and H184. These, and especially D183, are entirely conserved (including in bacterial PONs that are >70% diverged relative to mammalian PON1). Our previous studies indicated that residues 183-184 play no direct role in catalysis, but why these positions are so essential had remained unclear. It now seems that they play a primary role in aligning N168, which, in turn, ligates the catalytic Ca^{+2}. The computational simulations support this model. Specifically, we observed that changes in H2's configuration produce changes in the positioning of the D183-H184 dyad that, in turn, alter the interaction of N168 with the catalytic Ca^{+2}, and reduce the enzymatic activation energy. The simulations also explain a critical observation regarding the selectivity of HDL binding stimulation: only PON1's native lactonase activity is stimulated, whilst the promiscuous paraoxonase activity remains largely unaffected.

Our model, and the newly obtained crystal structure of rePON1-192Q, also account for the reduced HDL binding, stability and stimulation of human PON1-192Q relative to the 192R isozyme. The alterations to the hydrogen bonding network include, specifically, the appearance of a new interaction with F186's backbone carbonyl, and the tightening of the interaction with S166. It is clear that the structures of PON1, whereby the enzyme was purified and crystallized in detergent, do not reflect PON1's catalytically optimal configuration, which is only obtained upon binding to HDL. Thus, although no changes in backbone are observed with 192Q and R structures, the former may stabilize a suboptimal configuration. Indeed, MD simulations of the computational models of both the 192Q and 192R polymorphs, along with rePON1's 192K, indicated that, unlike 192Q, 192K/R interact extensively with both D183 and S166 (Sanan et al, 2010).

Finally, our results also rule out the alternative hypothesis, that Y71 mediates the effects of HDL binding. This despite the fact that Y71's hydroxyl appears to be H-bonded to D183 (Figure 3), and the cross-linking data that implicated it in HDL binding (Huang et al, 2013). The strongest point that contributes to elimination of this hypothesis is that the Y71G mutant shows stability comparable to that of wild type rePON1, and only marginally lower enzymatic stimulation (**Table S1**). Interestingly, analysis of this mutant in the presence of a detergent, tergitol, showed that while it had only a mild effect on the lactonase activity (~5-fold decrease with TBBL), the paraoxonase activity was markedly reduced (~120-fold decrease). Thus, although the highly flexible active-site loop at the tip of which Y71 resides plays a major role in substrate specificity (Ben-David et al, 2012), its effects seem to be HDL-independent.

This study also augments our limited knowledge of how lipid interactions modulate enzyme structure, catalytic efficiency and specificity. The enzymes best studied that show significant alteration of their activity upon binding to lipid membranes (interfacial activation) are lipases, and especially phospholipase A2 (PLA_2). The latter shares several features with PON1, such as the proximity of the active site to the membrane interface, and a highly mobile active-site loop. Analogously to the findings for PON1, truncation of the N- terminal helix of PLA_2 (Qin et al, 2004), or even point mutations, resulted in a significant decrease in both PLA_2's stability and activity (Chiou et al, 2008a; Chiou et al, 2008b). Also in resemblance to PON1, the N-terminal helix of PLA_2 (residues 1-12) shows high mobility in the lipid-free form (van den Berg et al, 1995). This configurational flexibility infiltrates to the active site, and specifically to the catalytic

residues H48 and D99 (van den Berg et al, 1995). It was, therefore, postulated that the lipid-bound PLA_2 adopts a fixed conformation that reinforces the hydrogen bonds between catalytic residues, resulting in efficient catalysis.

The revealed mechanism of PON1's interfacial activation is similar, although not in atomic details, since PLA_2 and PON1 differ in both their folds and their active-sites, but in the overall effect of reducing the enzyme's conformational ensemble, and aligning the key catalytic residues (N168, and the catalytic Ca^{+2}), thus producing lower activation energies and higher catalytic rates.

Beyond these specific cases of interfacial activation, it appears that active-site floppiness, *i.e.*, excess of mobility of active-site residues, is a challenge to enzyme catalysis. The coexistence of multiple sub-states is counter-productive with respect to rate acceleration, namely catalysis of the chemical step, as is seen in the effect of H2 mobility on PON1's enzymatic activation energy. Widening of the conformational ensemble may also account for the gradual loss of rate acceleration (k_{cat}/k_{uncat}) with increasing temperature, a loss that seems to occur in all enzymes, including thermophilic ones, and occurs within the range of temperatures in which the folded state is fully maintained. Active-site floppiness also seems to underline designed enzymes, where the conformation of key active-site residues is not sufficiently defined. In the course of the evolutionary optimization of computationally designed enzymes, such alternative configurations are minimized, but not completely eliminated (Elias et al, 2014; Giger et al, 2013; Khersonsky et al, 2012). Indeed, what designed active sites seem to be lacking most is the networks of interactions that align catalytic residues such N168 and the catalytic Ca^{+2} in PON1. These networks include second-shell residues (*e.g.* D183-H184) and third-shell residues (K192, S166 and H2 residues; **Figure S3**). The essentiality of this network is manifested in the fact that disturbance of even its most far-reaching periphery (absence of HDL interactions, or mutations in 192) results in rate declines of up to 20-fold, and disturbance of second-shell residues such as D183 leads to complete loss of activity.

Table S1: Stimulation of activity and rates of inactivation of wild-type-like rePON1 and its mutants.

Variant	Activity stimulation[b]			Inactivation[e]
	K_{app}(μM)[c]	V_{max} (%)[d]	V_{max}/K_{app} (μM^{-1})	Residual lactonase activity (%)[f]
rePON1	0.58±0.07 (1)	406±11 (1)	700±86 (1)	80±7 (1)
Δ20-rePON1	>10[g] (> ↓17)	---	---	20±6 (↓ 4)
Y185A	0.68±0.1 (↓ 1.2)	484±19 (↑ 1.2)	712±105 (1)	71±4 (↓ 1.1)
F186A	2.4±0.3 (↓ 4)	331±15 (↓ 1.2)	138±18 (↓ 5)	11±1 (↓ 7)
Y185A/F186A	2.9±0.7 (↓ 5)	183±17 (↓ 2.2)	63±16 (↓ 11)	6±2 (↓ 13)
Y185G	>10[g] (> ↓17)	---	---	15±3 (↓ 5)
F186G	1.5±0.4 (↓ 2.6)	159±13 (↓ 2.6)	106±30 (↓ 6.6)	7±1 (↓ 11)
Y190A	1.3±0.3 (↓ 2.2)	268±17 (↓ 1.5)	206±49 (↓ 3.4)	59±2 (↓ 1.4)
W194A	0.46±0.13 (↑ 1.3)	188±10 (↓ 2.2)	409±118 (↓ 1.7)	73±5 (↓ 1.1)
Y190A/W194A	3±1 (↓ 5.2)	152±18 (↓ 2.7)	51±18 (↓ 13.7)	36±1 (↓ 2.2)
L198A	2.2±0.2 (↓ 3.8)	518±19 (↑ 1.3)	259±23 (↓ 2.7)	47±6 (↓ 1.7)
Y71F	0.8±0.1 (↓ 1.4)	467±14 (↑ 1.2)	584±75 (↓ 1.2)	75±5 (↓ 1.1)
Y71G	1.70±0.09 (↓ 2.9)	430±7 (↑ 1.1)	253±14 (↓ 2.8)	73±6 (↓ 1.1)
H184Q	1.5±0.2 (↓ 2.6)	367±12 (↓ 1.1)	245±34 (↓ 2.9)	34±3 (↓ 2.4)
H184T	1.00±0.09 (↓ 1.7)	613±14 (↑ 1.5)	613±57 (↓ 1.1)	96±8 (↑ 1.2)

[a] The TBBL concentrations used in the activity stimulation and inactivation are 0.25mM and 0.5mM, respectively. [b] Stimulation of the lactonase activity of rePON1 by different concentrations of rHDL (0-10μM). [c] The apparent affinity for rHDL stimulation is the concentration of rHDL that results in half-maximal stimulation of the activity. [d] V_{max} values are presented as the percentage relative to the expression of rePON1 in the absence of rHDL. [e] Inactivation of rePON1 by EDTA (15mM). [f] The residual lactonase activity is presented as the percentage at 72 hr of incubation at 37°C relative to time zero.

[g] The reaction rates did not show saturation, and an upper limit for the K_{app} value was provided based on the maximal rHDL concentration used. In brackets is the fold decrease or increase relative to the wild-type-like rePON1.

Table S2: Summary of data collection and refinement statistics

Data Collection	**K192Q**
Resolution range (Å)[a]	40-2.3 (2.34-2.3)
Space group	$P4_32_12$
Unit Cell Dimensions (Å)	
a=b	93.5
c	144
Number of reflections measured	410,343
Number of unique reflections[a]	29,085 (1424)
R_{sym} [a]	0.125 (0.684)
Completeness (%)[a]	100 (100)
Redundancy[a]	14.1 (13.9)
<I> / <s (I) >[a]	27.7 (4.3)

[a] Values in parentheses are for the highest-resolution shell.

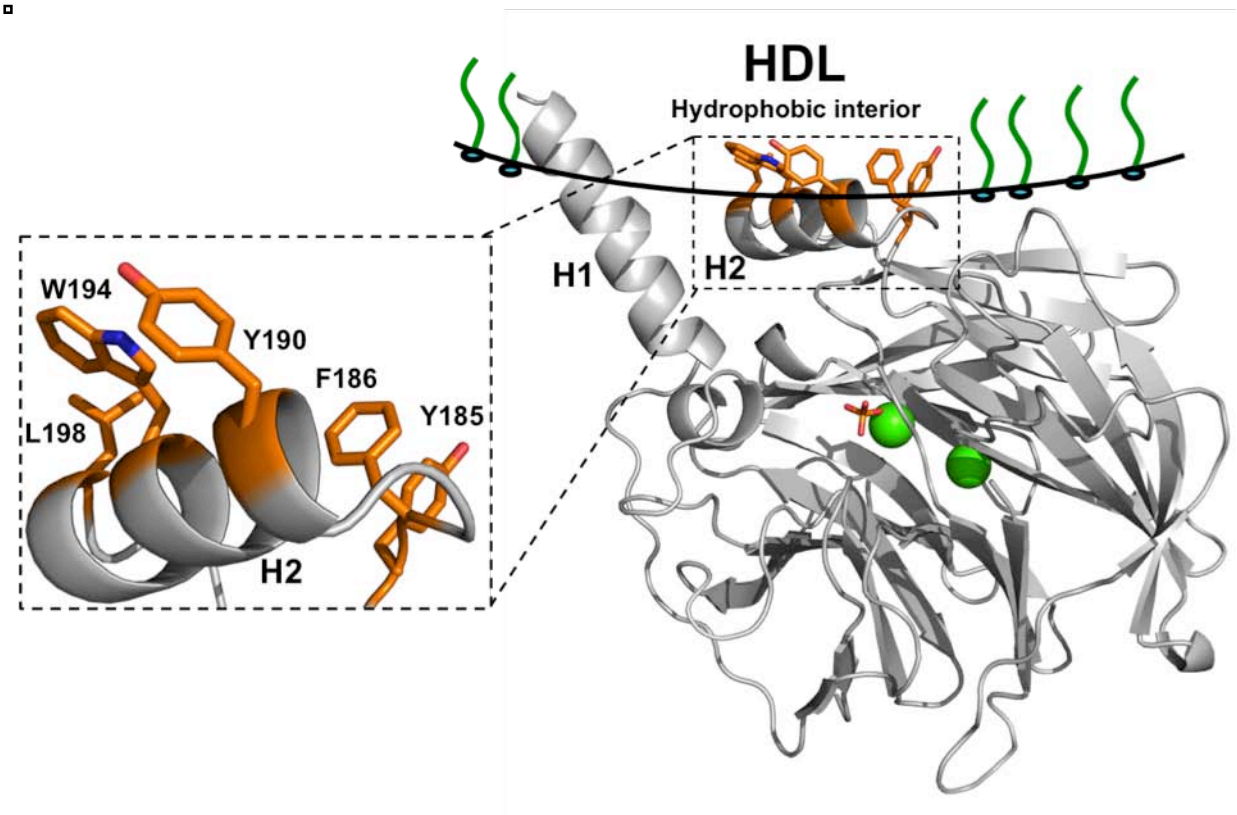

Figure S1: The proposed model for anchoring of PON1 to HDL based on the crystal structure of rePON1 (PDB code: 3SRE). This model suggests the interactions of PON1 helices H1 and H2 with the HDL surface. Hydrophobic residues that reside on helix H2, and on H2's C-terminal connecting loop, and are proposed to mediate anchoring to HDL are shown in *orange*.

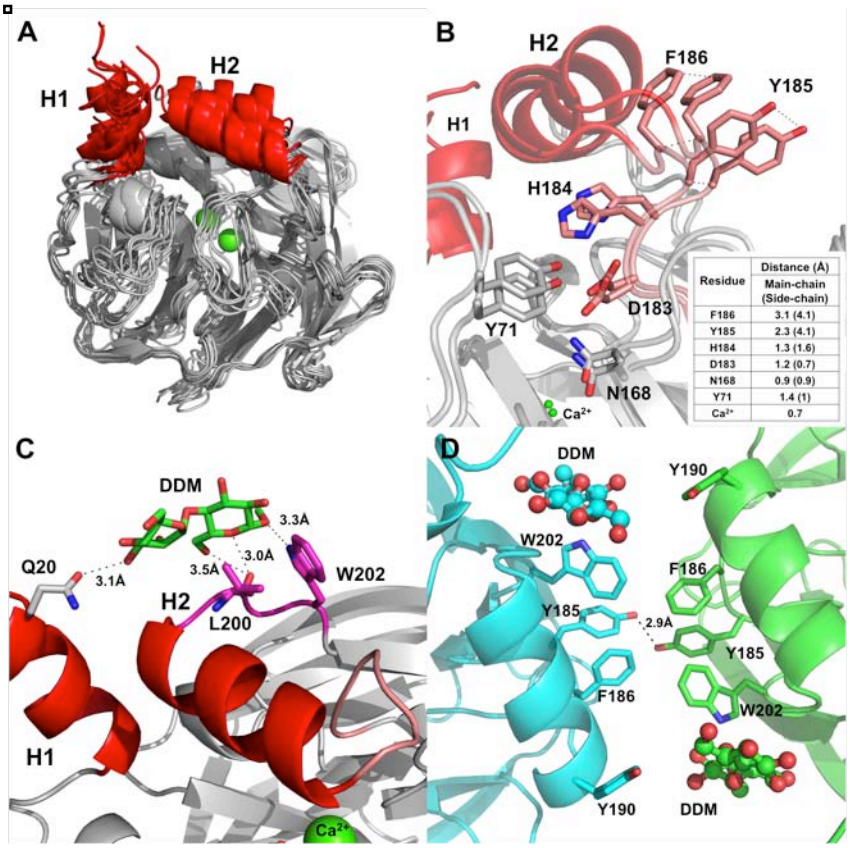

Figure S2: Structural properties of H1 and H2. The analysis was based on the wild-type-like rePON1 structure (PDB code: 3SRE).

A. Superposition of the normal modes, as predicted by *elNémo*, indicates the high mobility of helices H1 and H2 (in *red*).

B. The two edge normal mode configurations of H2 and its C-terminus connecting loop, including the side chains of H2's C-terminus loop residues Y185 and F186, and the adjacent active site residues, the D83-H184 dyad, the active-site mobile loop residue Y71, and N168 that ligates the catalytic calcium (green sphere). The inset lists the distances of main- and side-chains between these two extreme configurations.

C. A close view of the interactions of the observed part of a detergent molecule, *n*-dodecyl-beta-*D*-maltoside molecule, DDM (*green*; shown is the sugar moiety, the electron density for the lipophilic chain of DDM could not be defined). Shown also are the adjacent residues of H1 (*grey*) and of H2's N-terminal connecting loop (*magenta*).

D. View of the crystal packing interactions within different PON1 molecules (*green* and *cyan*) within unit cells of rePON1. Shown is the packing surface that involves interactions between the adjacent H2 helices and their C-terminal connecting loops.

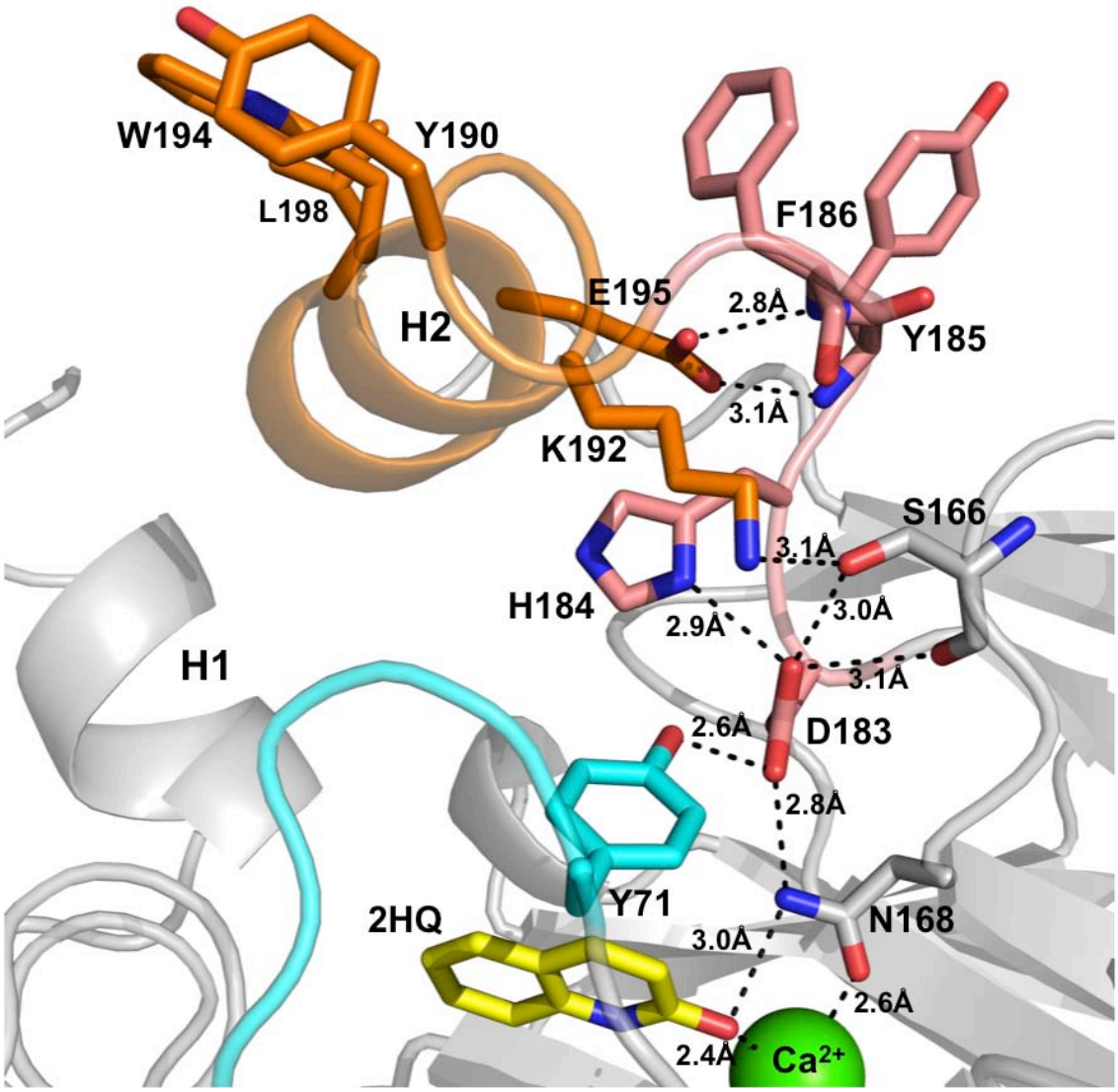

Figure S3: Interactions of residues D183 and H184 with first-shell active-site residues (PDB code: 3SRG). Depicted are putative hydrogen bonds of D183 and H184 to H2 residues (*orange*) and to its C-terminal loop (*salmon*), as well to the catalytic Ca^{+2}-ligating residue, N168 (*grey*). Shown is the lactone analogue 2-hydroxyquinoline (2HQ, in *yellow*) and Y71 that resides in an active-site mobile loop (*cyan*). Our model suggests that HDL binding results in the fixation of a well-defined conformation of H2 and of its C-terminal loop. Immobilization of these relatively floppy parts of the enzyme (**Figure 2**), results in the alignment of the D183-H184 dyad, of N168, and thereby of the catalytic Ca^{+2}, thus accounting for the dramatic increase in PON1's stability and lactonase activity when bound to HDL.

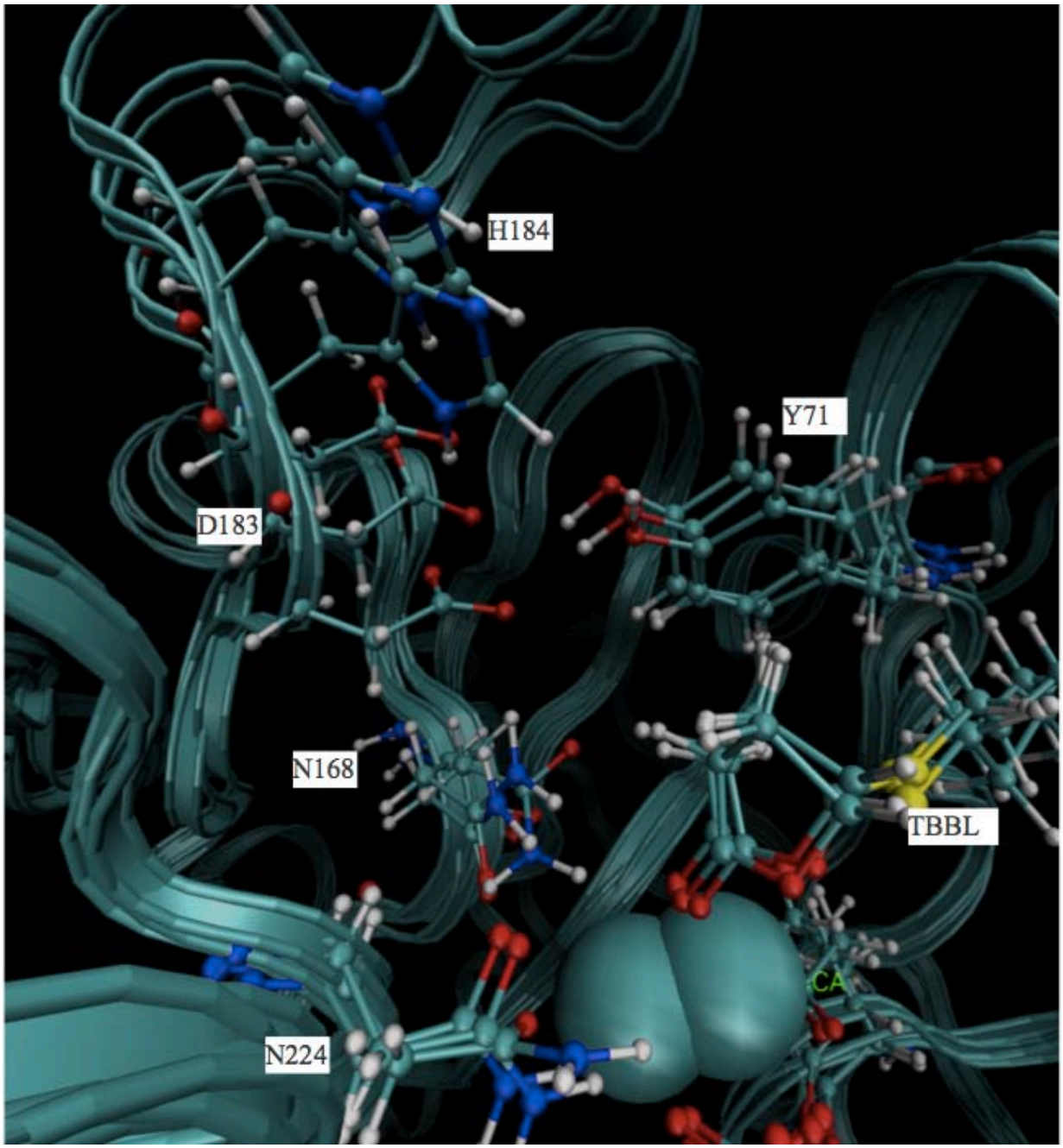

Figure S4: The effect of H2 adjustment on the active-site architecture and on substrate catalysis. Superimposition of the computational models with helix H2 positions 0 (*color-1*), 2 (*color-2*) and 4 (*color-3*), in the presence of TBBL (**A**) and paraoxon (**B**) Shown are remarkable changes in the positioning of D183, H184, N168 and N224, induced by the adjustment of helix H2, highlighting structural differences between the models produced with TBBL and with paraoxon.

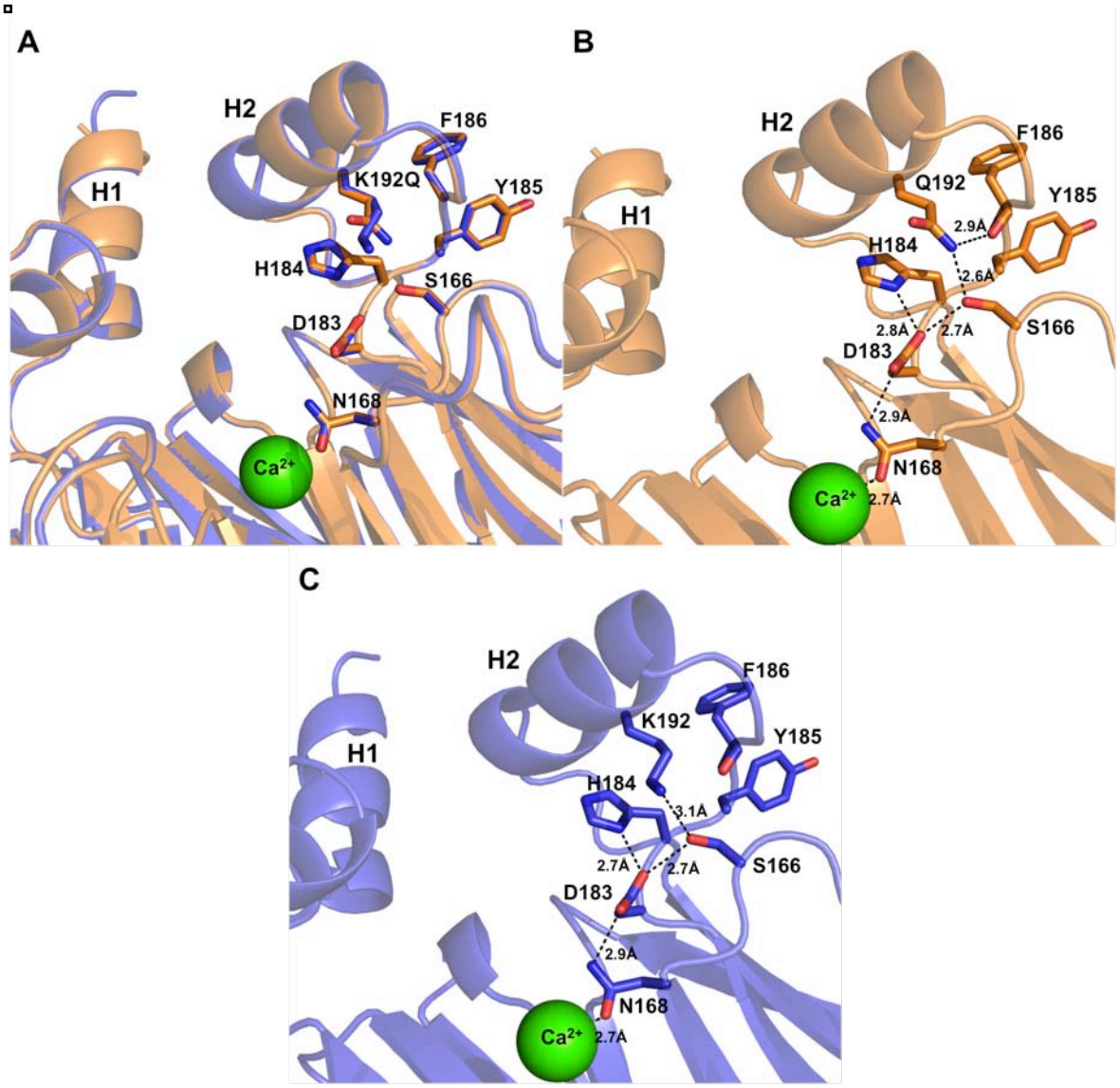

Figure S5: The crystal structure of rePON1-192Q. **A**. Overlay of rePON1-192K (PDB code: 3SRE; *blue*) with the newly solved structure of rePON1-192Q (*orange*). **B**. The network of putative hydrogen bonds spanning from H2 and its C-terminal loop, through D183, to the catalytic Ca^{+2}-ligating residue N168 in rePON1-192Q. **C**. The same analysis for rePON1-192K.

References (Supplementary part)

Aviram M, Vaya J (2013) Paraoxonase 1 activities, regulation, and interactions with atherosclerotic lesion. *Current opinion in lipidology* **24:** 339-344

Bar-Rogovsky H, Hugenmatter A, Tawfik DS (2013) The evolutionary origins of detoxifying enzymes: the mammalian serum paraoxonases (PONs) relate to bacterial homoserine lactonases. *The Journal of biological chemistry* **288:** 23914-23927

Ben-David M, Elias M, Filippi JJ, Dunach E, Silman I, Sussman JL, Tawfik DS (2012) Catalytic versatility and backups in enzyme active sites: The case of serum paraoxonase 1. *J Mol Biol* **418:** 181-196

Ben-David M, Wieczorek G, Elias M, Silman I, Sussman JL, Tawfik DS (2013) Catalytic Metal Ion Rearrangements Underline Promiscuity and Evolvability of a Metalloenzyme. *J Mol Biol* **425:** 1028-1038

Chiou YL, Cheng YC, Kao PH, Wang JJ, Chang LS (2008a) Mutations on the N-terminal region abolish differentially the enzymatic activity, membrane-damaging activity and cytotoxicity of Taiwan cobra phospholipase A2. *Toxicon* **51:** 270-279

Chiou YL, Lin SR, Chang LS (2008b) Mutations on N-terminal region of Taiwan cobra phospholipase A(2) result in structurally distorted effects. *J Pept Sci* **14:** 890-897

Costa LG, Giordano G, Cole TB, Marsillach J, Furlong CE (2013) Paraoxonase 1 (PON1) as a genetic determinant of susceptibility to organophosphate toxicity. *Toxicology* **307:** 115-122

Elias M, Wieczorek G, Rosenne S, Tawfik DS (2014) The universality of enzymatic rate-temperature dependency. *TIBS* **39:** 1-7

Gaidukov L, Rosenblat M, Aviram M, Tawfik DS (2006) The 192R/Q polymorphs of serum paraoxonase PON1 differ in HDL binding, lipolactonase stimulation, and cholesterol efflux. *J Lipid Res* **47:** 2492-2502

Gaidukov L, Tawfik DS (2005) High affinity, stability, and lactonase activity of serum paraoxonase PON1 anchored on HDL with ApoA-I. *Biochemistry* **44:** 11843-11854

Gaidukov L, Viji RI, Yacobson S, Rosenblat M, Aviram M, Tawfik DS (2010) ApoE induces serum paraoxonase PON1 activity and stability similar to ApoA-I. *Biochemistry* **49:** 532-538

Giger L, Caner S, Obexer R, Kast P, Baker D, Ban N, Hilvert D (2013) Evolution of a designed retro-aldolase leads to complete active site remodeling. *Nat Chem Biol* **9:** 494-498

Harel M, Aharoni A, Gaidukov L, Brumshtein B, Khersonsky O, Meged R, Dvir H, Ravelli RB, McCarthy A, Toker L, Silman I, Sussman JL, Tawfik DS (2004) Structure and evolution of the serum paraoxonase family of detoxifying and anti-atherosclerotic enzymes. *Nat Struct Mol Biol* **11:** 412-419

Huang Y, Wu Z, Riwanto M, Gao S, Levison BS, Gu X, Fu X, Wagner MA, Besler C, Gerstenecker G, Zhang R, Li XM, DiDonato AJ, Gogonea V, Tang WH, Smith JD, Plow EF, Fox PL, Shih DM, Lusis AJ, Fisher EA, DiDonato JA, Landmesser U, Hazen SL (2013) Myeloperoxidase, paraoxonase-1, and HDL form a functional ternary complex. *The Journal of clinical investigation* **123:** 3815-3828

Josse D, Xie W, Renault F, Rochu D, Schopfer LM, Masson P, Lockridge O (1999) Identification of residues essential for human paraoxonase (PON1) arylesterase/organophosphatase activities. *Biochemistry* **38:** 2816-2825

Khersonsky O, Kiss G, Rothlisberger D, Dym O, Albeck S, Houk KN, Baker D, Tawfik DS (2012) Bridging the gaps in design methodologies by evolutionary optimization of the stability and proficiency of designed Kemp eliminase KE59. *Proc Natl Acad Sci USA* **109:** 10358-10363

Khersonsky O, Tawfik DS (2006) The histidine 115-134 DYAD mediates the lactonase activity of mammalian serum paraoxonases. *J Biol Chem* **281:** 7649-7657

Kuo CL, La Du BN (1998) Calcium binding by human and rabbit serum paraoxonases. Structural stability and enzymatic activity. *Drug Metab Dispos* **26:** 653-660

Matthews BW, Nicholson H, Becktel WJ (1987) Enhanced protein thermostability from site-directed mutations that decrease the entropy of unfolding. *Proceedings of the National Academy of Sciences of the United States of America* **84:** 6663-6667

Oda MN, Bielicki JK, Berger T, Forte TM (2001) Cysteine substitutions in apolipoprotein A-I primary structure modulate paraoxonase activity. *Biochemistry* **40:** 1710-1718

Qin S, Pande AH, Nemec KN, Tatulian SA (2004) The N-terminal alpha-helix of pancreatic phospholipase A2 determines productive-mode orientation of the enzyme at the membrane surface. *J Mol Biol* **344:** 71-89

Sanan TT, Muthukrishnan S, Beck JM, Tao P, Hayes CJ, Otto TC, Cerasoli DM, Lenz DE, Hadad CM (2010) Computational modeling of human paraoxonase 1: preparation of protein models, binding studies, and mechanistic insights. *Journal of Physical Organic Chemistry* **23:** 357-369

She ZG, Chen HZ, Yan Y, Li H, Liu DP (2012) The human paraoxonase gene cluster as a target in the treatment of atherosclerosis. *Antioxidants & redox signaling* **16:** 597-632

van den Berg B, Tessari M, Boelens R, Dijkman R, de Haas GH, Kaptein R, Verheij HM (1995) NMR structures of phospholipase A2 reveal conformational changes during interfacial activation. *Nat Struct Biol* **2:** 402-406